Predictions for gain in the fission-fragment-excited atomic xenon laser

Jong W. Shon and Mark J. Kushner[a)]
University of Illinois, Department of Electrical and Computer Engineering, 1406 W. Green Street, Urbana, Illinois 61801

Gregory A. Hebner and Gerald N. Hays
Sandia National Laboratories, Albuquerque, New Mexico 87185

(Received 30 June 1992; accepted for publication 1 December 1992)

The infrared atomic xenon laser ($5d \rightarrow 6p$) is an attractive candidate for fission fragment excitation, which provides low-power deposition (1–100 W cm^{-3}), long pulse lengths (1–10 ms), and high-energy deposition (100s J ℓ^{-1}). Optical gain at 1.73 and 2.03 μm has recently been measured in a reactor-excited xenon laser yielding values exceeding 0.03–0.05 cm^{-1} at power depositions of less than 10s W cm^{-3}. Gain was also found to rapidly terminate before the peak of the pump pulse for some experimental conditions. A computer model has been developed to predict gain in fission-fragment-excited xenon lasers and these experiments have been analyzed. It is found that the termination of gain is most likely attributable to gas heating which increases the electron density, leading to electron collision quenching. The specific dependence of gain on pump rate suggests that a reduced rate of recombination of molecular ions with increasing gas temperature is partly responsible for this behavior.

I. INTRODUCTION

During the past few years, there has been a renewed interest in the atomic xenon laser as an efficient source of infrared radiation. The atomic xenon laser is capable of operating at high efficiency ($\lesssim$5%) over a wide range of pump rates (10s W cm^{-3} to 10s kW cm^{-3}).[1–11] The gas mixtures typically contain a small fraction of xenon (less than a few percent) in rare-gas buffers at pressures of 0.5–5 atm. Various excitation methods have been used including electron-beam pumping,[2,5] electron-beam-sustained discharge,[6] self-sustained discharge,[7] microwave discharge,[8] and fission fragment excitation.[9–11]

The atomic xenon laser is most often operated on one or more of six infrared transitions between 1.73 and 3.65 μm corresponding to transitions between the $5d$ and $6p$ manifolds. Inversion mechanisms and the energy loading effects of the atomic xenon laser using Ar/Xe mixtures have been previously discussed in the context of electron-beam and fission fragment pumping.[12,13] In summary, excitation of the upper laser levels ($5d[3/2]_1$ and $5d[5/2]_2$) is believed to occur as a result of a collisional-radiative cascade following dissociative recombination of $ArXe^+$ and electron-impact excitation from Xe($6s$).[12] (See Fig. 1.) The depopulation of the lower laser levels ($6p[1/2]_0$, $6p[3/2]_1$, $6p[5/2]_2$) occurs by radiative relaxation or collisional quenching by heavy particles to the $6s$ levels. The intrinsic efficiency of Ar/Xe laser, measured as high as 5%, is comparable to the quantum efficiency of the 1.73 μm transition, which is $\approx$7%. An explanation of this phenomenon was first proposed by Lawton *et al.*[1] and Basov *et al.*[2] as being the recirculation of xenon atoms by electron-impact ionization from the $6s$ or higher levels to Xe($5d$) and Xe^+, followed by association reactions forming $ArXe^+$. This provides for a much more efficient path than direct electron-impact excitation of the ground state of xenon. This recirculation has been called electroionization.[1–3] The quantum efficiency based on the electroionization cycle is $\approx$30%. Results from our model of the xenon laser indicate that 20–30% of Xe^+ is formed by electron impact of Xe($6s$) and Xe($6s'$), with a comparable amount of excitation occurring from Xe($6s$) and Xe($6s'$) to higher excited states.

The selective nature of heavy particle quenching of the Xe($6p$) manifold by different buffer gases explains, in part, the spectrum of the laser output in a broadband optical cavity.[9,11] The 1.73, 2.03, and 2.65 μm Xe transitions share a common upper laser level. Therefore, as a first-order approximation, the dominant wavelength is determined by the quenching of the lower laser level. In Ar/Xe gas mixtures, the common lower laser level of the 1.73 and 2.63 μm transitions ($6p[5/2]_2$) is quenched by argon sufficiently fast so that both lines may simultaneously oscillate at the expense of the 2.03 μm transition whose lower laser level ($6p[3/2]_1$) is not strongly quenched. In helium buffered gas mixtures, helium preferentially quenches the lower level of the 2.03 μm transition, initiating a cascade which ultimately populates the lower level of the 1.73 μm transition.[11] The 2.03 μm transition also has a higher oscillator strength than the 1.73 μm transition. These conditions allow the 2.03 μm transition to oscillate in He/Ar/Xe mixtures having only 5%–20% of helium in a broadband optical cavity.[7,11]

Due to the high oscillator strengths of the laser transitions and a close match between the electron temperature and energy separation between the laser levels, the performance of the atomic xenon laser is sensitive to the effects of electron collision mixing (ECM).[12] We have previously proposed that at high power or energy loading, ECM thermalizes the laser levels and terminates oscillation when the fractional ionization exceeds a few 10^{-6}–10^{-5}, depending on the gas pressure and power deposition. The effects of

a)Author to whom correspondence should be addressed.

 0021-8979/93/062686-09$06.00

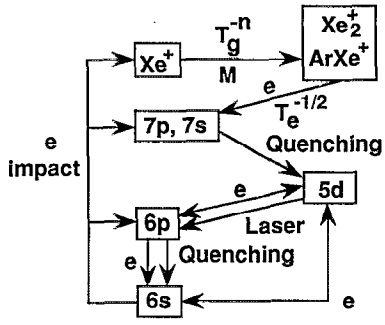

FIG. 1. Schematic of the inversion mechanism showing significant kinetic pathways in the Xe laser in Ar/Xe mixtures. Xe^+ forms Xe_2^+ and $ArXe^+$ through three-body association reactions. Dissociative recombination populates excited states of Xe which by a collisional radiative cascade pump the upper laser levels [Xe($5d$)]. Electron collision mixing of the Xe($5d$) and Xe($6p$); and electron-impact excitation from the Xe($6s$) contribute towards reducing gain at high pump powers and energy deposition.

high-energy loading, or gas heating, are also related to ECM. At a constant pump rate, increasing the gas temperature increases the electron density as a result of decreasing rates of dissociative recombination of the dimer ions.[12] Therefore, laser performance may degrade at a constant pump rate when gas heating increases the electron density above a critical value.

A compilation of the experimental results from a number of different systems using different pumping mechanisms has shown that the saturation intensity of the xenon laser scales as $P^{0.6}$, where P is the specific power deposition.[12] The implication of these results is that broadening of the transition is predominantly a result of electron collisions since the electron density scales roughly as $P^{0.5}$ in recombination-dominated plasmas. Unfortunately the combined effects of increased rates of excitation of the upper laser level, and increased mixing of the laser levels with increasing pump rates (electron density) complicate the interpretation of both experimental and theoretical results. For example, the saturation intensity of the xenon laser at low pump rates is only 10s W cm^{-2}. This results in the laser operating highly saturated under most conditions. Comparing laser output power between model and experiment therefore does not independently yield information on either saturation intensity or gain. This results from the fact that under highly saturated conditions, laser power scales as $g_0 I_s$ (g_0 is the small signal gain, I_s is the saturation intensity). Recently, however, direct measurements of gain at 1.73 and 2.03 μm have been made in a fission-fragment-excited atomic xenon laser operating at low pump power ($\leqslant$10s W cm^{-3}) at near-atmospheric pressure.[14,15] These measurements, combined with computer modeling, have enabled us to refine our understanding of the kinetics of the atomic xenon laser.

In this article, gain and broadening of the 1.73 and 2.03 μm transitions of the atomic xenon laser using rare-gas buffers are investigated using a computer model. Results from the model are compared to experimental measurements of gain made in fission-fragment-excited Ar/Xe, Ar/He/Xe, and Ar/Ne/Xe gas mixtures. The pumping mechanisms used in the model have been validated by comparing results of the model for laser power to experiments under saturated conditions. The comparisons made here therefore provide an opportunity to test predictions of broadening coefficients and other kinetics parameters[12] such as the effects of gas heating, pump rate, and gas pressure at low pump rates. In this work, we found that products of the quenching of the Xe($6p[3/2]_1$) level by argon must remain in the $6p$ manifold, as opposed to directly branching to the $6s$ levels, in order to explain the onset of absorption at high-energy loadings. Our results also suggest that the temperature dependence of three-body association reactions must also scale moderately with gas temperature ($T_g^{-1.5}$) to reproduce experimentally observed absorption at the laser wavelengths.

The computer model and experiments used in this study are described in Sec. II. Quantities derived from the model are discussed in Sec. III, followed by a comparison of computed and experimental values of gain for Ar/Xe, He/Ar/Xe, and Ne/Ar/Xe mixtures in Sec. IV. Scaling laws for the relation between gain, pump power, and energy deposition are proposed in Sec. V, followed by our concluding remarks in Sec. VI.

II. DESCRIPTION OF MODEL AND EXPERIMENT

The basic components of our computer model for the fission fragment excited laser have been previously discussed in Refs. 11–13, and therefore will be only briefly described here. The model is conceptually similar to models for particle-beam-excited excimer lasers. Additional levels of the rare gas are included to resolve the laser transitions. Eight levels in the $5d$ manifold and six levels in the $6p$ manifold of xenon are included in addition to the $6s$ and $6s'$ levels, a combined $7s/7p$ state, and a lumped excited state located at 11.5 eV representing radiating levels at higher energies. A listing of other species and reactions in the model can be found in Refs. 11 and 12. The model includes five laser transitions between the $5d$ and $6p$ manifolds: 1.73, 2.03, 2.63, 2.65, and 3.37 μm. The collisional broadening of these transitions by heavy particles and electrons is assumed to produce Lorentzian line shapes.

In fission fragment excitation, the plasma is generated by the slowing of energetic heavy ions in the laser gas mixture. In these experiments, described below, the heavy ions are produced by the fissioning of uranium foils lining the laser cavity. The ions are produced with two characteristic energies averaging 99 and 68 MeV. The heavy ions predominantly slow by ionizing the gas which generates energetic secondary electrons, which also ionize and excite the gas.

The model includes a calculation of the W values (energy deposition/event) for ionization and excitation of all levels of each component of the gas mixture by the heavy ions. This calculation is performed with a Monte Carlo simulation for the injected particles and secondary electrons[16] for individual gas mixtures. This calculation is necessary since W values are not simple functions of the gas mixture when the ionization potentials of the constituents are markedly different. Although these W values are cal-

culated based on electron-beam excitation, previous work has shown that W values for heavy ions differ by only 10% from those for electrons, and are usually larger.[17]

Since the pumping pulse in the fission-fragment-excited system of interest is approximately 2–10 ms long, a direct time-dependent calculation of the gain is computationally impractical. Therefore, model predictions were made at discrete points in the pump profile, integrating the rate equations for each species to their quasi-steady-state values (which are reached in 5–15 μs). The initial conditions for each of these discrete calculations include the gas temperature and power deposition, which is corrected for the gas motion. The gas temperature was calculated based on the integrated energy deposition in the gas to the time of interest. This latter assumption is only an approximation since calculations of the power deposition and hydrodynamics of the gain cell show that there is some gas motion into cool, unpumped regions.[18]

The dominant sources of ionization in particle-beam-excited plasmas are impact of ground-state species by the injected particles and energy energetic secondary electrons. These sources do not directly depend on the bulk electron temperature T_e. The electron temperature does, however, impact the kinetics since quenching, recombination, and multistep ionization rates are dependent on its value. In electron-beam-excited gas mixtures, the electron temperature is determined by the energy at which electrons recombine or attach. In rare-gas–halogen-gas mixtures where attachment is the dominant loss mechanism, the rate of electron loss is only a weak function of plasma density, and hence power deposition. In rare-gas mixtures, recombination is the dominant loss mechanism. Therefore, the rate of electron loss is proportional to plasma density, which in turn depends on power deposition.

We determined the electron temperature by using a Monte Carlo simulation (MCS) while including collisions with excited states and ions for a given gas mixture.[16] We parameterized the MCS to obtain a table of T_e as a function of excited state, electron densities, and gas mixture. This table was then interpolated during the actual calculation. Examples of these results for Ar/Xe and He/Ar/Xe mixtures are shown in Fig. 2. T_e is lower in He-buffered mixtures compared to Ar/Xe mixtures due to the larger rate of momentum transfer afforded by the lighter He. In all cases, T_e increases with increasing fractional ionization since the rate of recombination increases with the square of the fractional ionization, and recombination preferentially depletes the lower part of the electron energy distribution. These results are therefore analogous to the heating of the electron distribution which occurs when using large mole fractions of a thermal electron attaching gas such as F_2.[16] Although low-powered particle-beam-excited plasmas are often thought of as having rather cool temperatures, at fractional ionizations exceeding 10^{-5} the temperature can exceed 1 eV. This value is commensurate with those found in e-beam-pumped rare-gas halogen gas mixtures.

Briefly, the experiments were conducted using the Sandia Pulsed Reactor III (SPR III). The experimental apparatus is described in detail in Refs. 9, 11, and 19–21. The

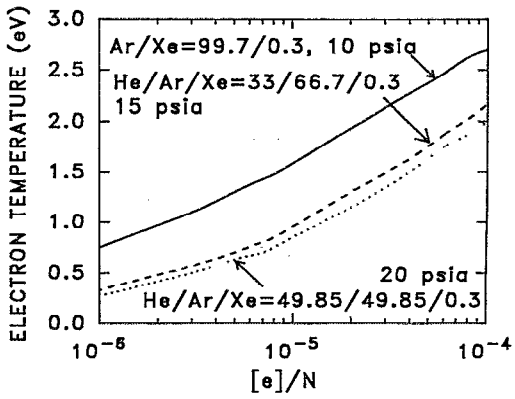

FIG. 2. Predicted electron temperature as a function of fractional ionization ($[e]/N$) for Ar/Xe and He/Ar/Xe gas mixtures. As the electron density increases, removal of low-energy electrons by recombination affectively heats the distribution.

active pumped volume of the laser cell is $60\times1\times7$ cm^3 and the cell is equipped with Brewster angle windows made of quartz. Fission fragments from the $^{235}UO_2$ foils lining the cavity are generated by neutron pulses from the reactor having pulse lengths of 0.5–5 ms full width at half-maximum (FWHM). The power deposition is obtained by normalizing the thermal neutron signals observed with a Reuter–Stokes cobalt detector to the energy deposition obtained by pressure rise. The pressure rise was corrected for thermally generated gas motion into unpumped regions of the cell as predicted by solving the Navier–Stokes equations for the convective gas motion.[18] These corrections increased the power deposition by 25%–40% compared to the value one would obtain from the pressure rise alone. Gain was measured using a F-center laser operating at 1.73 μm or a longitudinally excited electric discharge He/Xe laser operating at 2.03 μm.[22] A detailed discussion of the experimentally measured small signal gain as a function of gas mixture, pressure, and pump power will be presented elsewhere.[22]

III. DERIVED RATE COEFFICIENTS AND PROCESSES

A. Broadening rate coefficients

Predictions of laser power and intrinsic laser efficiency have been previously validated based on comparisons of our model's results with experiments performed on electron-beam-excited and fission-fragment-excited lasers.[11,12] Based on these comparisons, our proposed kinetic population mechanisms, including the effects of gas heating and ECM, have some credence. The predicted saturated output power is proportional to $g_0 I_s$. This value is somewhat independent of broadening since g_0 is inversely proportional to the broadening of the transition ($\Delta\nu$) while I_s is proportional to that broadening. Therefore, to first order, a kinetically consistent broadening coefficient for the laser transitions cannot be validated from comparisons based on laser power or energy; validation requires independent measurements of gain. The collisional broadening coefficients for the 1.73,[15,19] 3.36,[23] and 3.5 μm (Ref. 24)

TABLE I. Collisional broadening coefficients for Xe($5d[3/2]_1 - 6p[3/2]_1$).

Collision partner	Value derived from model ($cm^3 s^{-1}$)	Experimental value ($cm^3 s^{-1}$) (Refs. 15 and 19)
He	4.0×10^{-10}	6.5×10^{-10}
Ne	5.0×10^{-10}	5.0×10^{-10}
Ar	8.0×10^{-10}	6.2×10^{-10}

transitions have been reported by others. A subset of those broadening coefficients is shown in Table I.

The values of the pressure broadening rate coefficients for 1.73 μm transition used in the model were obtained by normalizing the predicted gain to the maximum value obtained in the experiments. The broadening coefficients so obtained are also shown in Table I. They differ from experimental values by less than 20%, except for the helium. The derived broadening coefficients in helium are lower by approximately half than those of the experiment. We attribute this to the fact that the electron density and electron temperature are closely coupled. Increases of the electron temperature of a few tenths of an eV can increase the electron density by a factor of 2. The total broadening is the result of both heavy particle and electron collisions, the latter which also quenches the inversion. Small uncertainties in the electron temperature therefore ultimately affect our derived broadening coefficients by heavy particles.

Although this procedure was sufficient to reproduce the maximum experimental gain for a variety of gas mixtures and pump rates, agreement could not be obtained over the entire length of the pulse without considering other kinetic processes.

B. Energy loading and gas temperature effects

Experiments by Voinov *et al.*[25,26] on the fission-pumped Ar/Xe laser showed that the laser output reached a maximum prior to the maximum of the pumping pulse. Similar trends have been observed by Hebner and Hays[14,15] for laser power and for laser gain, as discussed in this article. The gain and laser power deviate from being proportional to the power deposition, very often decreasing and the gain turning to absorption before the pump pulse reaches a maximum. Vionov *et al.*[25] proposed that the premature termination of the laser power results from disruption of the optical quality of the gas. Calculations and experiments were performed on the optical quality of our laser gas mixtures during reactor pumping.[27] The results indicated that the optical homogeneity is not significantly degraded for the pump rates and pressures of interest. For our conditions, the degradation in gain most likely results from energy loading, a rise in gas temperature, and a coincident rise in electron density. We have previously proposed that laser oscillation in the Xe laser is quenched by electron collision mixing of the laser levels when the electron density increases above a critical fractional ionization

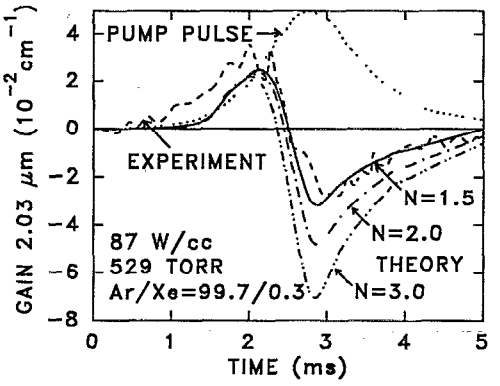

FIG. 3. Predictions for gain using different temperature dependencies for the rate coefficient for three-body ion association reactions. The experimental conditions are Ar/Xe=99.7/0.3, 529 Torr, peak pump power 87 W cm^{-3}. The rate coefficient scales as T_g^{-N}, and three trials are shown: $N=1.5$, 2.0, and 3.0. Agreement with experiment is obtained for $N\simeq1.5$.

of 5×10^{-6}–10^{-5}.[12] If the mixing is sufficiently large, the termination of laser oscillation, and gain, may be followed by absorption.

The sensitivity of laser performance to gas temperature is tied to the effects of ECM. In rare-gas mixtures, the electron density is determined by a balance between ionization and recombination. At a constant power deposition, the rate of ionization is independent of gas temperature. For this system the loss of electrons is dominated by dissociative recombination of dimer ions. The rate coefficient for association of dimer ions, a three-body process, scales approximately as T_g^{-N}.[28] Rate coefficients for dissociative recombination also decrease with increasing temperature. As a result, the electron density increases with increasing gas temperature due to there being a decreased density of dimer ions (relative to monomer ions) that recombine more slowly, even though the source due to ionization is constant.

We performed a parametric survey with our model in which we investigated the temperature dependence of a variety of heavy particle processes. We determined that the time (corresponding to a given energy loading or gas temperature) at which gain terminates is most sensitive to the temperature dependence of the three-body association reactions for forming dimer ions. The important reactions in Ar/Xe mixtures are $Ar^+ + Ar + M \rightarrow Ar_2^+ + M$, $Xe^+ + Ar + M \rightarrow ArXe^+ + M$, and $Xe^+ + Xe + M \rightarrow Xe_2^+ + M$. Measurements and theoretical studies of this process for a variety of ions have yielded dependencies of $T_g^{-0.5}$–$T_g^{-2.5}$. Typical results from our parametric survey in which we varied the temperature dependence of ion association reactions (T_g^{-N}, $1.5 \leqslant N \leqslant 3.0$) are shown in Fig. 3. We plotted our predictions with experimental results for gain at 2.03 μm in a fission-fragment-excited Ar/Xe=99.7/0.3 gas mixture. The gas pressure was 530 Torr and the maximum power deposition was 87 W cm^{-3}. The peak gain is well reproduced for all temperature dependencies, that is, for all values of N. The transition to, and magnitude of, the absorption, however, are sensitive to the temperature de-

TABLE II. Quenching rate coefficients for Xe(6p) Used in the model ($cm^3 s^{-1}$).

	Collision partner		
Xe(6p)	He[a]	Ne[a]	Ar[b]
$[1/2]_0$	6.0×10^{-12}	3.4×10^{-11}	1.4×10^{-10}
$[3/2]_2$	1.7×10^{-12}	4.7×10^{-13}	3.8×10^{-11}
$[3/2]_1$	7.49×10^{-11}	2.0×10^{-13}	1.1×10^{-11}
$[5/2]_3$	1.0×10^{-11}	3.0×10^{-12}	3.5×10^{-11}
$[5/2]_2$	9.2×10^{-12}	6.6×10^{-12}	1.0×10^{-10}
$[1/2]_1$	4.0×10^{-11}	3.0×10^{-12}	6.5×10^{-12}

[a]See Ref. 30.
[b]See Ref. 24.

pendence of dimer ion association ($T_g \simeq 550$ K at maximum absorption). We reproduce experimental results with a temperature dependence of $T_g^{-1.5}$. The underprediction of gain at the leading edge of the pulse is discussed below.

C. Effects of branching of heavy particle quenching of Xe(6p)

The high efficiency of the atomic Xe laser is partly due to the rapid depopulation of Xe(6p) manifold (lower laser levels) to other levels in the Xe(6p) manifold or to the 6s manifold by collisional quenching by argon and helium. Out of the seven infrared transitions between the 5d and 6p manifold, only one laser line is usually dominant, either the 1.73 or 2.03 μm line. This behavior is due, in part, to gain saturation and, in part, to selective quenching of the lower laser levels of the 1.73 and 2.03 μm transitions by argon and helium, respectively. Quenching rate constants and primary product state assignments have been reported for the deactivation of Xe(6p) states in Ar using one-photon excitation in the afterglow of a pulsed discharge and two-photon excitation in a static cell.[29–31] The quenching rate coefficients used in the model for Xe(6p) levels are shown in Table II. Quenching of the 6p and 5d manifolds of xenon may also occur by three-body collisions. Analysis of the molecular potentials and curve crossing for Xe_2^* suggests that three-body collisions of Xe atoms in the 5d manifold with ground-state xenon do not result in dimerization but predissociate to Xe(6s). A similar process is likely to occur for the higher levels of Xe(6p), while the lower levels of Xe(6p), Xe(6p'), and Xe(6s) most likely dimerize.

The validity of these quenching coefficients and their branchings in the context of our model are obviously important factors in predicting gain. For example, at the beginning of our study, the total rate coefficients for quenching of Xe(6p) by Ar had been measured; however, their branchings were not known. If one proposes that the branchings of the quenching of Xe(6$p[3/2]_2$) are exclusively to Xe(6s) levels, as in quenching by xenon, the predicted gain (trace A in Fig. 4) decreases at the same time as observed in the experiments. However, the peak gain is larger than experiments and absorption is not predicted. If, instead, branching are to other levels in the 6p manifold, as later recommended in Ref. 29, the predictions for gain are in good agreement with the experiment. These results imply that the onset of absorption results, at least in part, from a bottlenecking of density in the Xe(6p) manifold. Bottlenecking in the lower laser manifold coupled with ECM with the Xe(5s) manifold thermalizes the laser levels, terminates the gain, and may result in absorption.

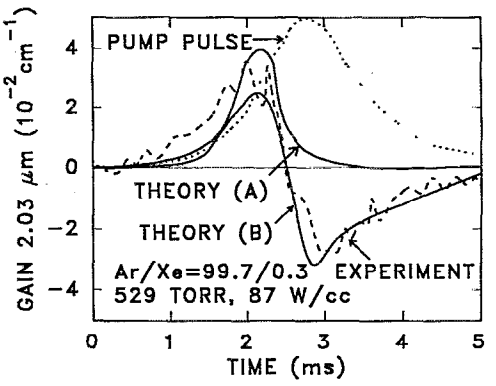

FIG. 4. Predictions for gain using different branchings for products of the quencing of Xe(6p). The conditions are the same as in Fig. 3. Theory A has branchings of the quenching to the Xe(6s) manifold. Theory B has branchings that are retained in the Xe(6p) manifold.

The uniqueness of the parameters we have derived in this exercise is certainly an issue. One could hypothesize other processes that will reproduce the experimental results. Given, however, the uncertainties in the reactor experiments, uncertainties in the existing database of rate coefficients, and the good agreement we have obtained between our model and experimental results, we believe our reaction scheme captures the essential physics while not necessarily being unique.

IV. ANALYSIS OF GAIN FOR Ar/Xe, He/Ar/Xe, AND Ne/Ar/Xe MIXTURES

Predictions of gain compared to experiment for the 2.03 μm transition in Ar/Xe=99.7/0.3 mixtures are shown in Figs. 5 and 6. The initial gas pressure was approximately 530 Torr and the maximum power deposition is approximately 87 W cm^{-3}. The peak gain and the onset

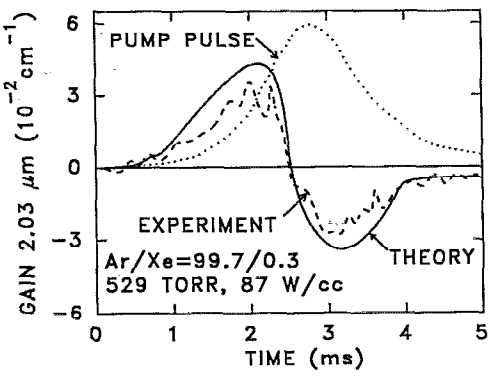

FIG. 5. Predicted and experimental gain, and pump power as a function of time for the 2.03 μm transition. The conditions are Ar/Xe=99.7/0.3, peak pump power 87 W cm^{-3}, and 529 Torr.

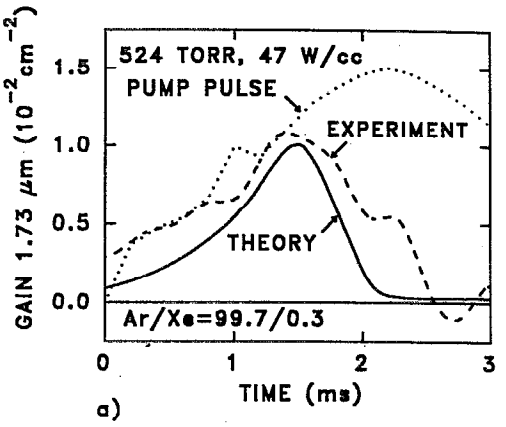

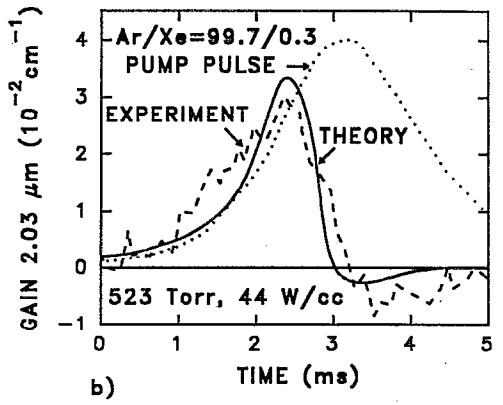

FIG. 6. Predicted and experimental gain, and pump power as a function of time for the 1.73 and 2.03 μm transitions in Ar/Xe=99.7/0.3. The conditions are (a) 1.73 μm, 47 W cm^{-3}, 524 Torr; (b) 2.03 μm, 44 W cm^{-3}, 523 Torr. Gain at 1.73 μm is 0.3–0.5 that at 2.03 μm.

of absorption are reproduced. The peak gain occurs prior to the maximum pump rate, while the absorption increases with increasing pump rates. The reason for the cutoff and onset of absorption is thermalization of the laser levels ($5d$ and $6p$ manifolds) resulting from electron-collision mixing and some additional amount of excitation from Xe($6s$) to Xe($6p$). The higher pump rate not only results in a higher electron density but also higher gas temperatures which, for the reasons discussed above, increases the electron density to even a larger value.

The predictions for gain shown in Fig. 5 differ from those in Fig. 3 at the leading edge of the pump pulse. Our model had underpredicted gain in the leading edge of the pump pulse where power deposition is <10 W cm^{-3}. The fact that experimental measurements of gain at the leading edge were unexpectedly high prompted a reexamination of the response of the thermal neutron detector at low pump powers. At low neutron flux, the cobalt detector is sensitive to the gamma ray flash produced by the reactor. This exercise resulted in a renormalization of the detector response, increasing the implied power deposition by approximately a factor of 2 at values <10 W. With this renormalization, the agreement with experiment is markedly improved.

Additional comparisons of predictions of gain with experiments for both the 1.73 and 2.03 μm transitions in an Ar/Xe=99.7/0.3 mixture are shown in Fig. 6. The initial gas pressure was $\approx$520 Torr and the maximum power deposition was $\approx$44–50 W cm^{-3}. Gains at 1.73 and 2.03 μm were measured on different reactor pulses. The dynamics of the SPR III reactor results in lower peak power pulses having longer pulse lengths. The peak gain occurs prior to the peak pump power for both the 2.03 and 1.73 μm transitions. The peak gain with a maximum pump power of 87 W cm^{-3} occurs at approximately 46 W cm^{-3} whereas that at a peak pump power of 44 W cm^{-3} occurs at approximately 33 W cm^{-3}. The values of the peak gain, approximately 0.03 cm^{-1}, are almost the same in both cases. Since the pulse length at the lower pump rate is somewhat longer, the onset of absorption occurs at almost identical amounts of energy deposition, approximately 45–50 J/ℓ.

The predicted and experimental gain at 1.73 μm have peak values of approximately 0.01 cm^{-1}. In general, gain on the 1.73 μm transition is 0.3–0.5 that of the 2.03 μm transition in spite of the higher rate of quenching of the lower laser level of the 1.73 μm. This indicates that bottlenecking in the lower level ($6p[5/2]_2$), at least prior to cutoff, is not a limiting factor. The higher gain at 2.03 μm is largely a result of the higher oscillator strength for that transition.

Comparisons of gain for a He/Ar/Xe mixture are shown in Fig. 7 for 1.73 and 2.03 μm lines, respectively. The gas mixture is He/Ar/Xe=49.4/50.3/0.3 at a total pressure of 1034 Torr with peak pumping powers of 50–60 W cm^{-3}. The trends are similar to that for the Ar/Xe mixtures, except that the gain on the 2.03 μm transition is, on a relative basis, larger than the 1.73 μm due to the more favorable rate of quenching of its lower laser level by He. The predicted peak gain for 2.03 μm agrees well with experiment while that for 1.73 μm is 10%–20% lower than that obtained in the experiments. The predicted values are quite sensitive to small changes in electron temperature and power deposition, as explained in the previous section. Due to the higher heat capacity resulting from adding helium, the gas heating that causes the cutoff of the gain is reduced, allowing the gain pulse to nearly track the pumping pulse. Peak gain still occurs somewhat prior to the peak of the pump pulse though the onset of absorption is significantly delayed, if it occurs at all. The specific energy deposition at which absorption occurs is approximately 80 J/ℓ atm, somewhat larger than that for the Ar/Xe mixtures, which is approximately 68 J/ℓ atm.

Comparisons of the model and experimental results for gain at 2.03 μm in a Ne/Ar/Xe=33/66.7/0.3 gas mixture are shown in Fig. 8. The peak pump power is 30 W cm^{-3} and initial gas pressure is 776 Torr. The gain is comparable to that obtained in He/Ar/Xe mixtures. Gain also prematurely peaks in this mixture; however, the added heat capacity provided by the addition of Ne to the mixture lengthens the gain pulse to nearly the entire duration of the pumping pulse (100 J/ℓ atm). We found from results of the model that the gain in Ne/Ar/Xe mixtures is quite sensitive to the rate of Penning ionization of Xe ions by

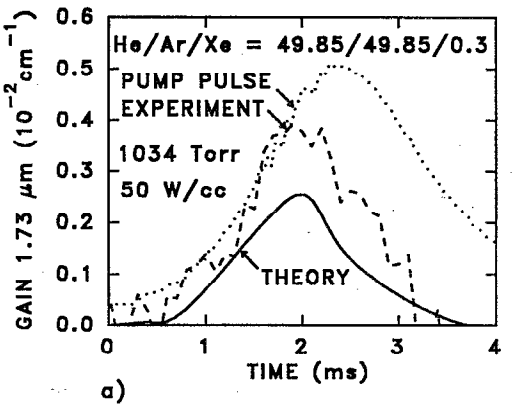

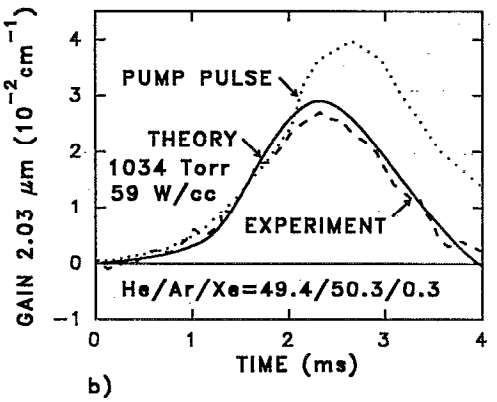

FIG. 7. Predicted and experimental gain, and pump power as a function of time for the 1.73 and 2.03 μm transitions. The conditions are (a) 1.73 μm, He/Ar/Xe=49.85/49.85/0.3, pump power 50 W cm^{-3}, and 1034 Torr; (b) 2.03 μm, He/Ar/Xe=49.4/50.3/0.3, pump power 59 W cm^{-3}, and 1034 Torr. The lower specific energy deposition allows gain to extend to longer times.

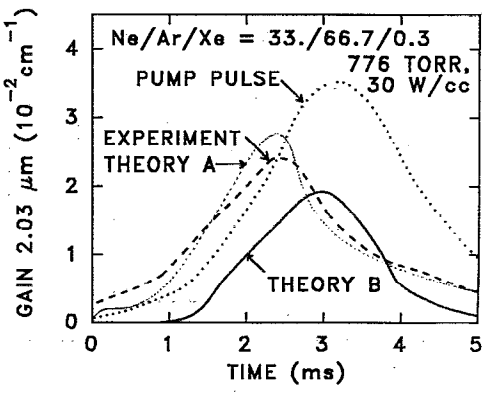

FIG. 8. Predicted and experimental gain, and pump power as a function of time for the 2.03 μm transition. The conditions are Ne/Ar/Xe=33/66.7/0.3, pump power 30 W cm^{-3}, and 776 Torr. Two theoretical curves are shown. Curve A uses a rate coefficient for Penning ionization of Xe by Ne-excited states of 2×10^{-10} cm^3 s^{-1}. Curve B uses a rate coefficient of 1×10^{-11} cm^3 s^{-1}.

Ne-excited states. The curve labeled A in Fig. 8 was obtained using a rate coefficient of 2×10^{-10} cm^3 s^{-1} for this Penning process, while the curve labeled B was obtained using a rate coefficient of 1×10^{-11} cm^3 s^{-1}. Since Ne is not a particularly rapid, nor selective, quencher of Xe($6p$), the addition of Ne to the gas mixture can only decrease gain by intercepting power that would otherwise channel to the upper laser levels. A rapid transfer of excitation between Ne and Xe, particularly Xe ions, prevents parasitic processes such as formation of Ne dimers and radiative relaxation, from decreasing the inversion density.

V. SCALING OF XENON LASER

Similar gains in the Xe laser are obtained at similar specific power and energy depositions. For example, gains from three separate experiments are plotted in Fig. 9 for different Ne/Ar/Xe mixtures: Ne/Ar/Xe=33.3/66.4/0.3, 0.286 atm, 39 W cm^{-3}; 66.5/33.3/0.2, 0.381 atm, 43 W cm^{-3}; Ne/Ar/Xe 74.4/24.5/0.1, 0.572 atm, 46 W cm^{-3}. The diameter of the circles in Fig. 9 represents the relative magnitude of gain, whereas the location of the circles corresponds to the power and energy deposition of that particular experiment. Within experimental uncertainties, similar gains are obtained at similar locations in the specific power (W/cm^3 atm) and specific energy deposition (J/cm^3 atm) parameter space. Unfortunately, the experiments are restrictured to nearly the same trajectory in the power-energy deposition plane since the shape of the pumping pulse is not easily controlled in reactor experiments.

To alleviate this restriction and to derive scaling laws for the Xe laser, the following computer experiments were performed. The gains at 1.73 and 2.03 μm were calculated for a variety of gas mixtures while independently varying the power and energy deposition. The range of values in the survey were $5\leqslant P$ (W/cm^3)$\leqslant 30$ and $50\leqslant E$ (mJ/cm^3)$\leqslant 150$. We restricted ourselves to conditions that correspond to being prior to the cutoff observed in gain. We then searched for a scaling parameter based on the logic that increased pump power increases gain whereas as increasing energy deposition decreases gain due to gas heating. This lead to the general form $g_0 \sim P/(E+b)^c$ where b and c are constants. The results of that survey are shown in Fig. 10. Circles and triangles are results from the model from a variety of combinations of P and E. The lines are the proposed scaling laws.

We found that in Ar/Xe mixtures (0.69 atm), the data was fit well by g_0 (10^{-2} cm^{-1})$=P/(E+100)^{0.8}$ at 1.73 μm, and $P/(E+100)^{0.5}$ at 2.03 μm. The characteristic energy deposition for reduction in the gain is then approximately 50 J/ℓ atm, or a temperature rise of approximately 100 K. Although the gain at 1.73 μm is lower than 2.03 μm, it appears to be less sensitive to energy deposition than is the 2.03 μm transition, as born out by the experimental results in Fig. 9. Similar gain scalings were obtained for He/Ar/Xe mixtures (0.69 atm), as shown in Fig. 10(b). The scaling relationship we derived is $g_0 \simeq P/(E+100)^{0.8}$. These scaling relationships are valid for P and E prior to the premature cutoff in gain.

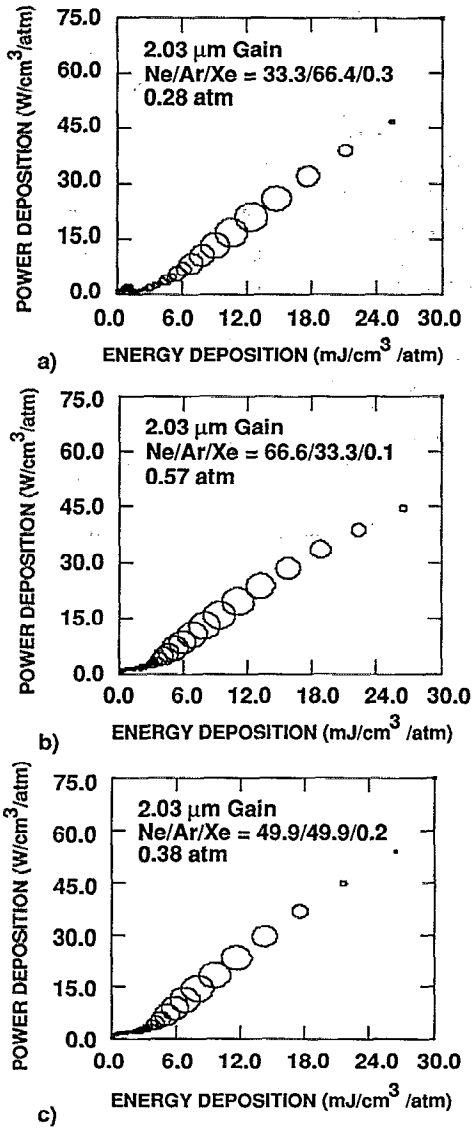

FIG. 9. Experimental gain (2.03 μm transition) plotted in terms of power and energy deposition. Size of the circles represents the relative magnitude in gain: (a) Ne/Ar/Xe=33.3/66.4/0.3, 0.286 atm, 39 W/cm^3; (b) Ne/Ar/Xe=74.4/24.5/0.1, 0.572 atm, 46 W/cm^3; (c) Ne/Ar/Xe =66.5/33.3/0.2, 0.381 atm, 43 W/cm^3.

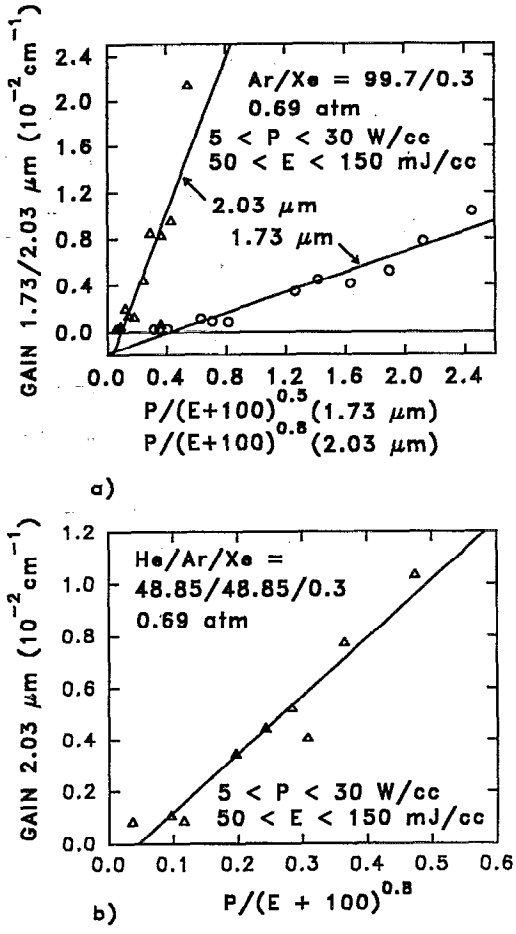

FIG. 10. Results from computer experiments for gain over a range of power deposition [5$\leq P$ (W/cm^3)$\leq$30] and energy deposition [50$\leq E$ (mJ/cm^3)$\leq$150]. (a) 1.73 and 2.03 μm transitions for Ar/Xe mixtures. (b) 2.03 μm transition for He/Ar/Xe mixtures. Gain scalings of the form $g_0 \approx P/(E+b)^c$ are suggested. The symbols are for trials performed at different combinations of P and E.

VI. CONCLUDING REMARKS

Gain predictions for the xenon laser from a plasma kinetics computer model have been presented and compared with experiments from fission fragment excitation of Ar/Xe, He/Ar/Xe, and Ne/Ar/Xe mixtures. Gain predictions at pump powers of 10s W cm^{-3} and energy loadings of 10s mJ cm^{-3} agree well with experiments. We determined that the products of quenching of Xe($6p$) levels by Ar likely remain in the $6p$ manifold. We also derived an effective gas temperature dependence for three-body ion association reactions, $T_g^{-3/2}$. Scaling laws were proposed for low-power, high-energy deposition pumping of the xenon laser prior to the cutoff in gain. The proposed scaling law is $P/(E+100)^n$, were P is specific power deposition (W/cm^3 atm) and E is specific energy deposition (mJ/cm^3 atm). These scalings reflect that gain increases with increasing pump rate but decreases with increasing energy deposition due to the effects of gas heating.

ACKNOWLEDGMENTS

The authors would like to thank W. J. Alford and E. L. Patterson of Sandia National Laboratories for numerous discussions and access to their experimental results prior to publication. This work was supported by Sandia National Laboratories and the National Science Foundation (ECS91-02326, CTS91-13215).

[1] S. A. Lawton, J. B. Richards, L. A. Newman, L. Specht, and T. A. DeTemple, J. Appl. Phys. **50**, 3888 (1979).
[2] N. G. Basov, V. A. Danilychev, A. Yu. Dudin, D. A. Zayarnyl, N. N. Ustinovsky, I. V. Kholin, and A. Y. Chugunov, Sov. J. Quantum Electron. **14**, 1158 (1984).
[3] N. G. Basov, V. V. Baranov, A. Y. Chugunov, V. A. Danilychev, A. Yu. Dudin, I. V. Kholin, N. N. Ustinovsky, and D. A. Zayarnyi, IEEE J. Quantum Electron. **QE-21**, 1756 (1985).
[4] A. Suda, B. Wexler, B. Feldman, and K. Riley, Appl. Phys. Lett. **54**, 1305 (1989).

[5] A. Suda, B. L. Wexler, K. J. Riley, and B. J. Feldman, IEEE J. Quantum Electron. **QE-26**, 911 (1990).
[6] A. Suda, B. L. Wexler, K. J. Riley, and B. J. Feldman, IEEE J. Quantum Electron. **QE-26**, 1304 (1990).
[7] K. Komatsu, E. Matsui, F. Kannari, and M. Obara, IEEE J. Quantum Electron. **QE-27**, 90 (1991).
[8] C. L. Gordon III, B. Feldman, and C. P. Christensen, Opt. Lett. **13**, 114 (1988).
[9] W. J. Alford and G. N. Hays, J. Appl. Phys. **65**, 3760 (1989).
[10] E. L. Patterson, G. E. Samlin, P. J. Brannon, and M. J. Hurst, IEEE J. Quantum Electron. **QE-26**, 1661 (1990).
[11] W. J. Alford, G. N. Hays, M. Ohwa, and M. J. Kushner, J. Appl. Phys. **69**, 1843 (1990).
[12] M. Ohwa, T. J. Moratz, and M. J. Kushner, J. Appl. Phys. **66**, 5131 (1989).
[13] M. Ohwa and M. J. Kushner, IEEE J. Quantum Electron. **QE-26**, 1639 (1990).
[14] G. A. Hebner and G. N. Hays, 43rd Gaseous Electronics Conference, Urbana, IL, October 1990, paper QB-1.
[15] G. A. Hebner and G. N. Hays, in *Conference on Lasers and Electro-optics* (Optical Society of America, Washington, DC, 1991), p. 516.
[16] M. J. Kushner, J. Appl. Phys. **66**, 2297 (1989).
[17] T. J. Moratz T. D. Saunders, and M. J. Kushner, J. Appl. Phys. **64**, 3799 (1988).
[18] J. Torczynski, Sandia National Laboratories, 1990 (unpublished).
[19] G. A. Hebner and G. N. Hays, Appl. Phys. Lett. **59**, 537 (1991).
[20] G. A. Hebner and G. N. Hays, Appl. Phys. Lett. **57**, 2175 (1990).
[21] G. A. Hebner and G. N. Hays, J. Appl. Phys. **71**, 1610 (1992).
[22] G. Hebner and G. N. Hays (to be published).
[23] R. Vetter and D. Reymann, J. Phys. B **7**, 323 (1974).
[24] J. Nella, S. Y. Szeto, P. Rabinowitz, and J. T. Latourrette, IEEE J. Quantum Electron. **QE-12**, 543 (1976).
[25] A. M. Voinov, L. E. Dovbysh, V. N. Krivonosov, S. P. Mel'nikov, I. V. Podmoshenskii, and A. A. Sinyanskii, Sov. Tech. Phys. Lett. **7**, 437 (1981).
[26] A. M. Voinov, L. E. Dovbysh, V. N. Krivonosov, S. P. Mel'nikov, I. V. Podmoshenskii, and A. A. Sinyanskii, Sov. Phys. Dokl. **24**, 189 (1979).
[27] D. R. Neal, J. R. Torcynski, W. J. Alford, R. B. Michie, and D. E. Bodette, in *Conference on Lasers and Electro-optics* (Optical Society of America, Washington, DC, 1991), pp. 244–245.
[28] R. Johnsen, J. Chem. Phys. **85**, 3869 (1986).
[29] J. Xu and D. W. Setser, J. Chem. Phys. **92**, 4191 (1990).
[30] J. Xu and D. W. Setser, J. Chem. Phys. **94**, 4243 (1991).
[31] W. J. Alford, IEEE J. Quantum Electron. **QE-26**, 1633 (1990).